

A Flow-Based Model for Conditional and Probabilistic Electricity Consumption Profile Generation and Prediction

Weijie Xia, *Student Member, IEEE*, Chenguang Wang, *Member, IEEE*, Peter Palensky, *Senior Member, IEEE*, Pedro P. Vergara, *Senior Member, IEEE*

Abstract—Residential Load Profile (RLP) generation and prediction are critical for the operation and planning of distribution networks, especially as diverse low-carbon technologies (e.g., photovoltaic and electric vehicles) are increasingly adopted. This paper introduces a novel flow-based generative model, termed Full Convolutional Profile Flow (FCPFlow), which is uniquely designed for both conditional and unconditional RLP generation, and for probabilistic load forecasting. By introducing two new layers—the invertible linear layer and the invertible normalization layer—the proposed FCPFlow architecture shows three main advantages compared to traditional statistical and contemporary deep generative models: 1) it is well-suited for RLP generation under continuous conditions, such as varying weather and annual electricity consumption, 2) it demonstrates superior scalability in different datasets compared to traditional statistical models, and 3) it also demonstrates better modeling capabilities in capturing the complex correlation of RLPs compared with deep generative models.

Index Terms—Load Profiles, Demand Profile, Generative Model, Forecast.

I. INTRODUCTION

RESIDENTIAL Load Profiles (RLPs) have wide applications in areas such as energy supply and demand management [1], modern distribution system planning [2], and risk analysis [3]. The validity of these studies depends largely on the quality of RLPs used. However, access to RLP data is limited due to privacy [4]. RLP generation can provide effective solutions to these problems. On the one hand, distribution system operators (DSOs) rely on RLPs for refining planning decisions. Historical data inaccessibility or limitations can hinder this process, yet the generation of RLPs provides system planners with an alternative to executing more informed planning [5]. For instance, in [6], generated RLPs were used to understand consumption patterns and optimize the system planning. On the other hand, generated RLPs can function as augmented data to support high-level tasks. For example, generated RLPs or PV profiles are used to support the training of models for load prediction [7], non-intrusive load monitoring algorithms [8], and reinforcement learning [9].

This research was supported by the Aling4Energy project (NWA.1389.20.251) and utilized the Dutch National e-Infrastructure with the support from the SURF Cooperative (grant number: EINF-5398).

Weijie Xia, Peter Palensky, and Pedro P. Vergara are with the Intelligent Electrical Power Grids (IEPG) Group, Delft University of Technology, 2628 CD Delft, The Netherlands (e-mail:{W.xia, PP.VergaraBarrios, P.Palensky}@tudelft.nl).

Chengunag Wang is with Alliander N.V., 6812 AH Arnhem, The Netherlands. e-mail: chenguang.wang@alliander.com;

Traditional RLP modeling primarily employs Gaussian Mixture Models (GMMs) [10], [11]. However, GMMs exhibit limited effectiveness in capturing the complexities of RLP distributions. An alternative approach involves using Copulas models. The study by [12] applies prominent multivariate Copulas models to simulate electric vehicle (EV) charging consumption profiles. Their findings indicate that t-Copulas outperform other functions in modeling these profiles. In recent years, the advancement of Machine Learning (ML) offers new approaches to RLP modeling. In [7], [13], [14], Generative adversarial networks (GANs) are used to either generate RLPs or PV profiles. In [15], Variational Auto-Encoder (VAE) is proposed to model EV charging profiles. In [16], a flow-based model is proposed for RLP generation that performs better in fitting peak and probability density functions than GANs. In [17], a hybrid model VAE-GAN is proposed for the synthesis of electrical load and PV generation data. The VAE-GAN is shown to possess greater modeling capabilities compared to using a standalone GAN model. In [18], a GAN-based generative model is introduced. This model focuses on privacy instead of generating accurate profiles, transforming real-world datasets into high-quality synthetic datasets that ensure user-level privacy. A study by [19] compared the performance of a convolutional Non-linear Independent Component Estimation (NICE) model with GANs in RLP generation. The findings indicate that the convolutional NICE model produces RLPs that exhibit smaller KL divergence relative to real data, suggesting a closer approximation to the actual RLP distributions. In [20], a MultiLoad-GAN was proposed, instead of generating individual RLP, MultiLoad-GAN generates a group of synthetic RLPs which essentially capture the spatial-temporal correlations among a group of loads.

Even though the above-mentioned methods show promising results, they do not include the effects of external factors on generated RLPs (such as weather information), which is becoming more important for state-of-the-art generation methods. Conditional generation is a solution to increase the manipulability of models. In [21], cWGANS are used for probabilistic load prediction, whereas GANs are used to assist a forecaster by generating residual scenarios. In [22], a ProfileSR-GAN is proposed to upsample low-resolution RLPs to high-resolution RLPs. Furthermore, it was observed that RLPs generated with the integration of weather information lead to better generation results based on the metrics used in

the research. In [23], a conditional VAE (cVAE) is proposed for representative scenario generation. In [24], two types of cVAE were employed for generating synthetic energy data. The findings from [24] suggest that including augmented data significantly enhanced building energy prediction, with accuracy improvements ranging between 12% and 18% during the experimental phase. In [25], a transferable flow-based generative model is proposed, which leverages RLP data of different households to improve the prediction of target households. In [26], a conditional MVT copula is proposed that outperforms conditional GMMs.

Despite these developments, current conditional generation methods face several challenges. 1) GANs-related models are effective with discrete conditions like days and seasons but perform poorly with continuous variables such as daily or annual consumption, temperature, and irradiation [27], [28]. Moreover, models such as GANs and VAEs struggle to replicate overall statistical features because they do not directly model probability densities [29]. Copulas models handle continuous conditions well [26], but their lack of scalability makes them impractical for large datasets or high-dimensional data. 3) Flow-based models avoid the above-mentioned limitations but suffer from inadequate modeling capabilities and slow convergence rates [30].

In this paper, we propose a new flow-based generative model architecture coined Full Convolutional Profile Flow (FCPFlow)¹, designed to address the three challenges previously discussed. The proposed FCPFlow architecture is built upon the idea of a classical flow-based model, proposed initially in [31], but designed to learn the features of RLP data efficiently. The key contributions of this paper are as follows:

- The proposed FCPFlow architecture is designed for RLP generation and probabilistic prediction. Through empirical and theoretical evaluation, FCPFlow demonstrates as main advantages: 1) Enhanced scalability over traditional statistical models (e.g., GMMs and Copulas), which depend on in advance defined hypotheses, offering more stable performance across various datasets. 2) Superior modeling performance based on selected evaluation metrics relative to other deep generative models, such as cNICE, cVAE, WGAN-GP, and cWGAN-GP.
- The proposed FCPFlow architecture is well-suited for RLP generation under continuous conditions (e.g., daily and annual consumption, weather information), which prior research has insufficiently addressed.

II. MODELING OF RESIDENTIAL LOAD PROFILES

In RLP modeling, a typical daily profile is split into T discrete time steps. For example, an RLP with a resolution of 15 minutes is characterized by a $T = 96$ time step (24 hours), while an RLP with a resolution of 30 minutes includes a $T = 48$ time step. Each time step corresponds to a specific value of active power consumption in these profiles. In general, an RLP profile can be described as a dataset

$$\mathcal{D} = \{\mathbf{x}_i\}_{i=1}^N = \{(x_{1,i}, \dots, x_{T,i})\}_{i=1}^N, \quad (1)$$

¹You can find the code, data, and other materials of this paper at <https://github.com/xiaowei1996/Full-Convolutional-Time-Series-Flow.git>

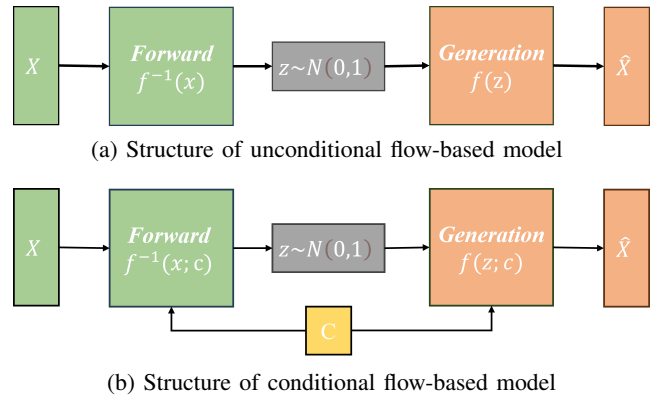


Fig. 1. Structure of flow-based models, where \mathbf{x} and $\hat{\mathbf{x}}$ are the input data and generated data, \mathbf{c} is the condition corresponding to data, \mathbf{z} is a latent variable following Gaussian distribution, and f is a bijective function $f : Z \rightarrow X$ which is usually constructed by NNs.

where $x_{t,i}$ is the active power consumption of t -th time step, $\mathbf{x}_i = (x_{1,i}, \dots, x_{T,i})$ represents one RLP. An unconditional deep generative model (e.g., GAN) can be trained to generate RLPs. Such a generative model can be expressed as $G_\theta(\mathbf{z}_i) = \mathbf{x}_i$, where $G(\cdot)$ is the generative model which maps \mathbf{z} to \mathbf{x} , θ is the learnable parameters, $\mathbf{z} \sim \pi(\mathbf{z})$, and $\pi(\mathbf{z})$ can be any simple distribution such as Gaussian distribution. Then, a conditional deep generative model can be expressed as

$$G_\theta(\mathbf{z}_i; \mathbf{c}_i) = \mathbf{x}_i, \quad (2)$$

where $\mathbf{c}_i = (c_{1,i}, \dots, c_{B,i})$ is the condition vector corresponding to the i -th RLP \mathbf{x}_i . In generative models, conditions can be imposed on the output of the generative model to influence the output outcome. For example, in Sec. VI-C, \mathbf{c}_i represents weather information; therefore, the ML model will generate weather-related RLPs.

III. BACKGROUND

A. Flow Based Models

The basic structure of conditional flow-based models is shown in Fig. 1, where f (usually constructed by neural networks (NNs)) is essentially the generator $G_\theta(\cdot)$ in (2) [30]. During training, function f^{-1} is learned to transform input data \mathbf{x} (with condition \mathbf{c}) into \mathbf{z} which follows a standard Gaussian distribution. Since the function f^{-1} is invertible, once f^{-1} is trained, its inverse f is used to take random samples \mathbf{z} (with condition \mathbf{c}) and generate \mathbf{x} . In flow-based models, function f (or f^{-1}) is usually constructed by stacking multiple invertible transformations f_i , meaning $f = f_1 \circ f_2 \dots \circ f_K$ and $f^{-1} = f_K^{-1} \circ f_{K-1}^{-1} \dots \circ f_1^{-1}$. Fig 2 demonstrates how this stacked function transforms a simple Gaussian distribution into data distribution $p_K(\mathbf{x}|\mathbf{c})$ and vice versa. By stacking invertible transformations f_i , the modeling capability of f is also increased, enabling function f to simulate more complex data distribution.

During the training process of a flow-based model, the model parameters can be obtained by maximizing the log-likelihood of the latent variable \mathbf{z} with respect to a standard

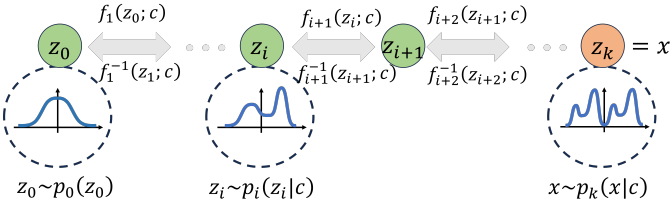


Fig. 2. Structure of a conditional flow-based model $f = f_1 \circ f_2 \dots \circ f_K$ which transform Gaussian distribution $p_0(\mathbf{z}_0)$ into complex target distribution $p_K(\mathbf{x}|\mathbf{c})$ [32] and vice versa.

Gaussian distribution. To do this, the *Change of Variable Theorem* is used, which is expressed as [33]

$$p_X(\mathbf{x}|\mathbf{c}) = p_Z(\mathbf{z}) \left| \det \left(\frac{\partial f^{-1}(\mathbf{x}; \mathbf{c})}{\partial \mathbf{x}} \right) \right|, \quad (3)$$

where \mathbf{x} is the input RLP data, \mathbf{c} is the condition (e.g., weather information), \mathbf{z} is a latent variable that follows a Gaussian distribution, p_X and p_Z are the distributions of \mathbf{x} and \mathbf{z} , respectively, and f is a bijective function $f : Z \rightarrow X$ which is usually constructed by NNs, $\det(\cdot)$ is the determinant function. The *Change of Variable Theorem* defines the relation between two distributions if there exists a bijective mapping $f : Z \rightarrow X$. Based on (3), the log-likelihood of $p_X(\mathbf{x}|\mathbf{c})$ can be expressed as

$$\log p_X(\mathbf{x}|\mathbf{c}) = \log p_Z(\mathbf{z}) + \log \left| \det \left(\frac{\partial f^{-1}(\mathbf{x}; \mathbf{c})}{\partial \mathbf{x}} \right) \right|. \quad (4)$$

However, as f is usually constructed by multiple transformations, i.e., $\mathbf{x} = f(\mathbf{z}; \mathbf{c}) = f_1 \circ f_2 \circ \dots \circ f_K(\mathbf{z}; \mathbf{c})$, expression (4) can be further written as

$$\log p_X(\mathbf{x}|\mathbf{c}) = \log p_Z(\mathbf{z}_0) + \sum_{j=1}^K \log \left| \det \left(\frac{\partial f_j^{-1}(\mathbf{z}_{j-1}; \mathbf{c})}{\partial \mathbf{z}_{j-1}} \right) \right|, \quad (5)$$

where $\mathbf{z}_j = f_j(\mathbf{z}_{j-1}; \mathbf{c})$ for $j = 1, \dots, K$ with $\mathbf{z}_K = \mathbf{x}$, and \mathbf{z}_i represents the intermediate latent variable at the i -th step of the transformation. Thus, the optimal model parameters $\hat{\theta}$ can be obtained by maximizing the log-likelihood of $p_X(\mathbf{x}|\mathbf{c})$, as

$$\hat{\theta} = \arg \max_{\theta} \log p_Z(\mathbf{z}_0) + \sum_{j=1}^K \log \left| \det \left(\frac{\partial f_j^{-1}(\mathbf{z}_{j-1}; \mathbf{c})}{\partial \mathbf{z}_{j-1}} \right) \right|. \quad (6)$$

B. Combining Coupling Layer

To guarantee that the transformation f_i is invertible when implemented through NNs, combining coupling layers can be used [34], denoted as f_{ccl} . Fig. 3 shows the structure of f_{ccl} and its inverse f_{ccl}^{-1} . The forward process of combining coupling layers f_{ccl}^{-1} can be expressed as

$$\mathbf{x}_1, \mathbf{x}_2 = \text{Split}(\mathbf{x}) \quad (7)$$

$$(\mathbf{x}_1, \mathbf{c}) = \text{Combine}(\mathbf{x}_1, \mathbf{c}) \quad (8)$$

$$\hat{\mathbf{z}}_1 = \exp(s_1(\mathbf{x}_1; \mathbf{c})) \odot \mathbf{x}_2 + t_1(\mathbf{x}_1; \mathbf{c}) \quad (9)$$

$$(\hat{\mathbf{z}}_1, \mathbf{c}) = \text{Combine}(\hat{\mathbf{z}}_1, \mathbf{c}) \quad (10)$$

$$\hat{\mathbf{z}}_2 = \exp(s_2(\hat{\mathbf{z}}_1; \mathbf{c})) \odot \mathbf{x}_1 + t_2(\hat{\mathbf{z}}_1; \mathbf{c}) \quad (11)$$

$$\hat{\mathbf{z}} = \text{Combine}(\hat{\mathbf{z}}_1, \hat{\mathbf{z}}_2), \quad (12)$$

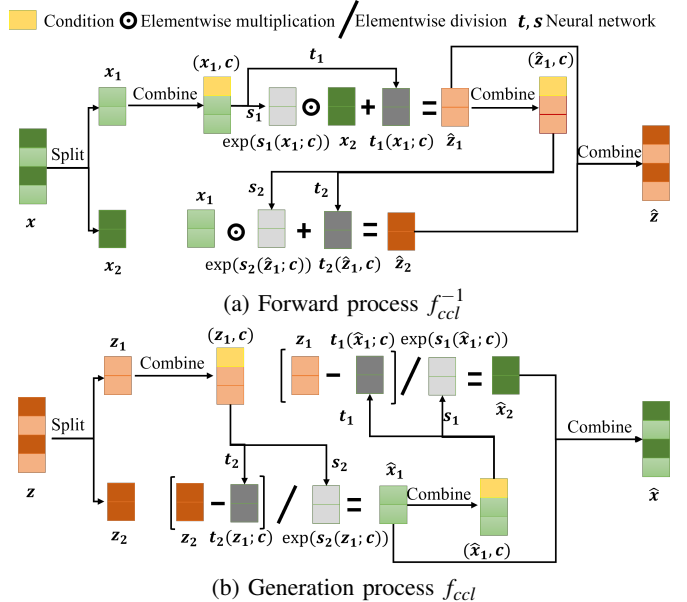


Fig. 3. The conditional transformation architecture of combining coupling layer f_{ccl} and its inverse. t and s are the neural networks that can be expressed as $t(\cdot)$ and $s(\cdot)$, both s and t reduce the input dimensions as demonstrated in the figure. \mathbf{x} and $\hat{\mathbf{x}}$ are the sampled and generated data, respectively. \mathbf{z} and $\hat{\mathbf{z}}$ are the sampled and generated latent variables, respectively.

where \mathbf{x} corresponds to the RLP data, the operation $\text{Split}(\cdot)$ partitions the input vector \mathbf{x} (or \mathbf{z}) into two sub-vectors \mathbf{x}_1 and \mathbf{x}_2 , corresponding to the even and odd elements of \mathbf{x} , s and t are NNs, $\text{Combine}(\cdot)$ refers to the method used to merge two vectors into a single vector, the symbol \odot indicates element-wise multiplication. The generation process of combining coupling layers f_{ccl} can be expressed as

$$\mathbf{z}_1, \mathbf{z}_2 = \text{Split}(\mathbf{z}) \quad (13)$$

$$(\mathbf{z}_1, \mathbf{c}) = \text{Combine}(\mathbf{z}_1, \mathbf{c}) \quad (14)$$

$$\hat{\mathbf{x}}_1 = (\mathbf{z}_2 - t_2(\mathbf{z}_1; \mathbf{c})) / \exp(s_2(\mathbf{z}_1; \mathbf{c})) \quad (15)$$

$$(\hat{\mathbf{x}}_1, \mathbf{c}) = \text{Combine}(\hat{\mathbf{x}}_1, \mathbf{c}) \quad (16)$$

$$\hat{\mathbf{x}}_2 = (\mathbf{z}_1 - t_1(\hat{\mathbf{x}}_1; \mathbf{c})) / \exp(s_1(\hat{\mathbf{x}}_1; \mathbf{c})) \quad (17)$$

$$\hat{\mathbf{x}} = \text{Combine}(\hat{\mathbf{x}}_1, \hat{\mathbf{x}}_2). \quad (18)$$

As previously discussed, to obtain the optimal set of parameters of NNs s and t , used to guarantee that transformation f_i is invertible, expression (5) can be used. To do this, the log-determinant of $\frac{\partial f_{ccl}^{-1}(\mathbf{x}; \mathbf{c})}{\partial \mathbf{x}^T}$ is needed, which can be expressed as

$$\begin{aligned} \log |\det \left(\frac{\partial f_{ccl}^{-1}(\mathbf{x}; \mathbf{c})}{\partial \mathbf{x}^T} \right)| &= \log |\det \left(\begin{matrix} \mathbb{I} & \mathbf{0} \\ * & \exp(s_2(\mathbf{z}_1; \mathbf{c})) \end{matrix} \right)| \\ &\quad + \log |\det \left(\begin{matrix} \mathbb{I} & \mathbf{0} \\ * & \exp(s_1(\mathbf{x}_1; \mathbf{c})) \end{matrix} \right)|, \end{aligned} \quad (19)$$

where \mathbb{I} is the identity matrix, the symbol $*$ denotes the elements in the lower-left quadrant. These elements are represented by $*$ since they do not influence the value of the log-determinant being considered. Consequently, the specific values of these elements are not of interest in this context and

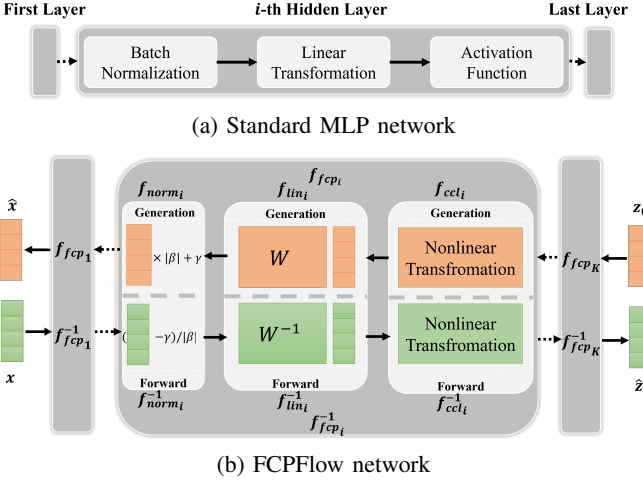


Fig. 4. FCPFlow architecture is structured to process data through a series of FCPFlow blocks. \mathbf{x} and $\hat{\mathbf{x}}$ are the sampled and generated RLPs, respectively. \mathbf{z}_0 and $\hat{\mathbf{z}}_0$ are the sampled and generated latent variables, respectively. β and γ are parameters in f_{norm_i} introduced in Sec. IV-A. W is a matrix that linearly transforms the input vector into another vector. W is introduced in Sec. IV-C.

thus are not explicitly specified. For the complete formulation, see [34].

Theoretically, by stacking combining coupling layer $f = f_{ccl_1} \circ f_{ccl_2} \circ \dots \circ f_{ccl_K}$, we can build a model that can simulate complex RLPs distribution $p(\mathbf{x}|\mathbf{c})$, thus enabling generation of conditioned RLPs. However, this modeling approach does not produce satisfactory results for time-series data. The reason is that the classical flow-based requires stacking many layers (with many parameters) to have sufficient modeling capabilities to be able to learn the complex distribution $p(\mathbf{x}|\mathbf{c})$. This brings two problems: 1) a significantly slow training process and 2) a need for large datasets to support the training process of large models. The proposed FCPFlow model addresses this issue when modeling RLP data while retaining the advantages of flow-based models.

IV. PROPOSED MODEL: FULL CONVOLUTIONAL PROFILE FLOW

The proposed architecture is composed of multiple FCPFlow blocks, denoted as f_{fcp_i} . At the same time, each f_{fcp_i} block is composed of three distinct components: an invertible normalization layer f_{norm_i} , an invertible linear layer f_{lin_i} , and a combining coupling layer f_{ccl_i} , as shown in Fig. 4. The introduction of f_{lin_i} and f_{norm_i} marks the difference from a traditional flow-based model, enriching the modeling capabilities of the FCPFlow architecture to handle time series data such as RLPs. Therefore, the operation of each transformation can be mathematically represented as a composition of these three layers: $f_{fcp_i} = f_{norm_i} \circ f_{lin_i} \circ f_{ccl_i}$. One FCPFlow model with K transformations can be expressed as $F^{fcp} = f_{fcp_1} \circ f_{fcp_2} \circ \dots \circ f_{fcp_K}$. Considering this, each FCPFlow block can be perfectly understood as an invertible counterpart to the traditional multilayer perception (MLP) as depicted in Fig. 4.

For each FCPFlow block, f_{fcp_i} , introduced in Sec. III, can be understood as an invertible nonlinear transformation

(with learnable parameters) that has the same function as the activation function in MLP. f_{norm_i} can be conceptualized as the invertible counterpart of the traditional batch normalization layer. This layer maintains dynamic mean and variance estimates throughout the training phase. Once the FCPFlow model is trained, these estimated parameters (mean and variance) are used in the forward and generation process. In parallel, f_{lin_i} is introduced as an invertible linear transformation layer characterized by learnable parameters W . During the forward operation, $f_{lin_i}^{-1}$ performs a linear mapping by applying matrix multiplication between W^{-1} and the layer's input. During the generation operation, f_{lin_i} mirrors this operation by using matrix W , thus maintaining the invertibility of the model and facilitating the generation process.

By introducing f_{norm_i} and f_{lin_i} , the proposed FCPFlow has higher modeling capabilities than classic flow-based RLP models. To achieve such capabilities, f_{norm_i} aims to stabilize the training process, while f_{lin_i} uses matrix W aiming to understand the correlations among individual time steps of the RLP data. By working with the nonlinear transformations provided by f_{ccl_i} , the proposed FCPFlow blocks can accurately describe the complex, high-dimensional correlations inherent in time series RLP data, addressing thus the classical flow-based models' limitations mentioned in Sec. III-B. To finalize the description of the proposed FCPFlow, the log-determinants of each layer are required. These are obtained as follows.

A. Invertible Normalization Layer

The functionality of the invertible normalization layer f_{norm_i} is presented in Fig. 4. This normalization operation can be mathematically expressed as in (20) and (21) for the forward and generation processes, respectively.

$$f_{norm}^{-1} \quad \mathbf{z} = \frac{\mathbf{x} - \gamma}{\sqrt{\beta^2 + \varepsilon}}, \quad (20)$$

$$f_{norm} \quad \mathbf{x} = \mathbf{z} \cdot \sqrt{\beta^2 + \varepsilon} + \gamma, \quad (21)$$

where γ and β are mean and standard deviation of \mathbf{x} and have the same shape as \mathbf{x} and \mathbf{z} , while ε is a small constant ensuring numerical stability.

To compute the log-likelihood, as expressed in (5), the log-determinant of the invertible normalization layer f_{norm} is required, which can be expressed as

$$\log |\det \left(\frac{\partial f_{norm}^{-1}(\mathbf{x})}{\partial \mathbf{x}^T} \right)| = -\log \left(\prod_{i=1}^T (|\beta_i| + \varepsilon) \right), \quad (22)$$

where T is the length of vector β , β_i denoting the i -th element of vector β , for $i \in 1, 2, \dots, T$.

B. Invertible Linear Layer

The operation of the invertible normalization layer, denoted as f_{lin_i} , is also presented in Fig. 4. The mathematical formalism for this layer's functionality, in the context of both forward and generative processes, is presented through (23) and (24), respectively.

$$f_{lin}^{-1} \quad \mathbf{z} = \mathbf{W}^{-1} \mathbf{x}, \quad (23)$$

$$f_{lin} \quad \mathbf{x} = \mathbf{W} \mathbf{z}, \quad (24)$$

TABLE I
DATASETS USED FOR THE MODEL COMPARISON.

Country	Resolution	Amount of RLPs
<i>Unconditional Generation</i>		
GE	15 minute	2,131
<i>Conditional Generation</i>		
NL	60 minute	27,757
AUS [35]	30 minute	10,000
UK	30 minute	10,000
USA [36]	15 minute	9,110
UK weather [37]	30 minute	10,000
<i>Load Prediction</i>		
NL	60 minute	365
UK	30 minute	365
USA [36]	15 minute	365

where \mathbf{W} is a invertible matrix. The log-determinants of the invertible linear layer f_{lin} is expressed as

$$\log |\det\left(\frac{df_{lin}^{-1}(\mathbf{x})}{d\mathbf{x}^T}\right)| = \log |\det(\mathbf{W}^{-1})|. \quad (25)$$

C. Maximum Likelihood Estimation of FCPFlow

Using the log-determinants of f_{lin_i} , f_{norm_i} , and f_{ccl_i} (described previously in Sec. III-B), the log-likelihood of a FCPFlow F^{fcl} model of K blocks can be expressed as

$$\begin{aligned} \log p_X(\mathbf{x}|\mathbf{c}) &= \log p_Z(\mathbf{z}_0) + \sum_{j=1}^K \left(\log \left| \det \left(\frac{\partial f_{ccl_j}^{-1}(\mathbf{z}_{j-1}; \mathbf{c})}{\partial \mathbf{z}_{j-1}^T} \right) \right| \right) \\ &= \log p_Z(\mathbf{z}_0) \\ &\quad + \sum_{j=1}^K \left(\log \left| \det \left(\frac{\partial f_{ccl_j}^{-1} \circ f_{lin_j}^{-1} \circ f_{norm_j}^{-1}(\mathbf{z}_{j-1}; \mathbf{c})}{\partial \mathbf{z}_{j-1}^T} \right) \right| \right). \end{aligned} \quad (26)$$

Given that the log-likelihood of F^{fcl} can be calculated using the expression in (26), it becomes feasible to train model F^{fcl} through the application of gradient descent maximizing such log-likelihood. In this case, the parameters subject to optimization include the parameters of matrices \mathbf{W}_i within f_{lin_i} , alongside the parameters of the NNs, denoted as s_i and t_i from f_{ccl_i} .

V. SIMULATIONS SETUP

A. Implementation Details

A notable challenge in training the proposed PCPFlow arises from using exponential and logarithmic functions in the combining coupling layers, which can lead to numerical instability. To mitigate this issue, we implement a soft clamping mechanism in combining coupling layers, as suggested by [34]. The trick is simply replacing $s(\mathbf{x}_i; \mathbf{c})$ with $s^{clamp}(\mathbf{x}_i; \mathbf{c})$, which is mathematically expressed as

$$s^{clamp}(\mathbf{x}_i; \mathbf{c}) = \frac{2\alpha}{\pi} \arctan\left(\frac{s(\mathbf{x}_i; \mathbf{c})}{\alpha}\right), \quad (27)$$

where α is a hyper-parameter, $s^{clamp}(\mathbf{x}_i; \mathbf{c}) \approx s(\mathbf{x}_i; \mathbf{c})$ for $|s(\mathbf{x}_i; \mathbf{c})| \ll \alpha$ and $s^{clamp}(\mathbf{x}_i; \mathbf{c}) \approx \pm\alpha$ for $\alpha \ll |s(\mathbf{x}_i; \mathbf{c})|$. $s^{clamp}(\mathbf{x}_i; \mathbf{c})$ can effectively curb the potential instabilities caused by the exponential function $\exp(s^{clamp}(\mathbf{x}_i; \mathbf{c}))$ [34]. Based on our experiment, the best range of α is $(0.1, 1)$.

B. Data Introduction

For a comprehensive comparison, RLP datasets from five countries were used. Table I outlines the details of these datasets. The UK, NL, and GE datasets sources can be found in our previous work [29]. The NL, UK, AUS, and USA datasets are used for conditional generation, in which the conditions are annual and daily total consumption in kWh. UK weather dataset is also used for the conditional generation, in which the conditions are different weather information (including cloud cover, sunshine, irradiation, maximum temperature, minimum temperature, mean temperature, pressure, and precipitation). The NL, UK, and USA datasets are also used for probabilistic prediction experiments. The number of RLPs in Table I refers to the amount of data used for the experiments. One RLP is defined as the consumption profile of a family for a day (with different time resolutions). For example, a one-week consumption profile for two households equals $7 \times 2 = 14$ RLPs.

C. Evaluation Metrics

1) *Evaluation Metrics for (conditional) RLP Generation:* Aligning with [23], [26], the evaluation metrics used in this paper from Section VI-A to VI-C are Energy Distance (ED), Maximum Mean Discrepancy (MMD), Wasserstein Distance (WD), KS Distance (KS), and MSE of Autocorrelation (MSE.A). The smaller the value of the above metrics, the better the performance of the model. The ED between two distributions P and Q can be represented as follows

$$D_E(P, Q) = 2\mathbb{E}\|\mathbf{x} - \mathbf{y}\| - \mathbb{E}\|\mathbf{x} - \mathbf{x}'\| - \mathbb{E}\|\mathbf{y} - \mathbf{y}'\| \quad (28)$$

where \mathbf{x} and \mathbf{x}' represent independent RLPs sampled from real distribution P , \mathbf{y} and \mathbf{y}' represent independent generated RLPs sampled from distribution Q (Q represents the distribution of generated RLPs). The KS between two empirical cumulative distribution functions (CDF) $F(\mathbf{x})$ and $F(\mathbf{y})$ is given by

$$D_{KS}(F(\mathbf{x}), F(\mathbf{y})) = \sup_{\mathbf{x}} |F(\mathbf{x}) - F(\mathbf{y})|, \quad (29)$$

where \sup denotes the supremum over all possible values of \mathbf{x} . For two sets of RLP datasets \mathcal{D}_1 and \mathcal{D}_2 , the MSE.A is computed as

$$\text{MSE} = \sum (R(\mathcal{D}_1) - R(\mathcal{D}_2))^2, \quad (30)$$

where $R(\mathcal{D}_1), R(\mathcal{D}_2)$ represent the autocorrelation of two datasets. The WD between two probability measures is defined as

$$W(P, Q) = \inf_{\pi \in \Pi(P, Q)} \int_{\mathbb{R}^d \times \mathbb{R}^d} \|\mathbf{x} - \mathbf{y}\| d\pi(\mathbf{x}, \mathbf{y}), \quad (31)$$

where $W(P, Q)$ is the WD between two distribution P and Q , \mathbf{x} and \mathbf{y} are RLPs sampled from P and Q . The MMD is expressed as

$$\text{MMD}(P, Q) = \sqrt{\mathbb{E}[k(x, x')] + \mathbb{E}[k(y, y')] - 2\mathbb{E}[k(x, y)]}, \quad (32)$$

where k is the Gaussian kernel $k(x, x') = \exp\left(-\frac{\|x-x'\|^2}{2\sigma^2}\right)$, \mathbf{x}, \mathbf{x}' are RLP samples in distribution P and \mathbf{y}, \mathbf{y}' are generated RLP samples in distribution Q .

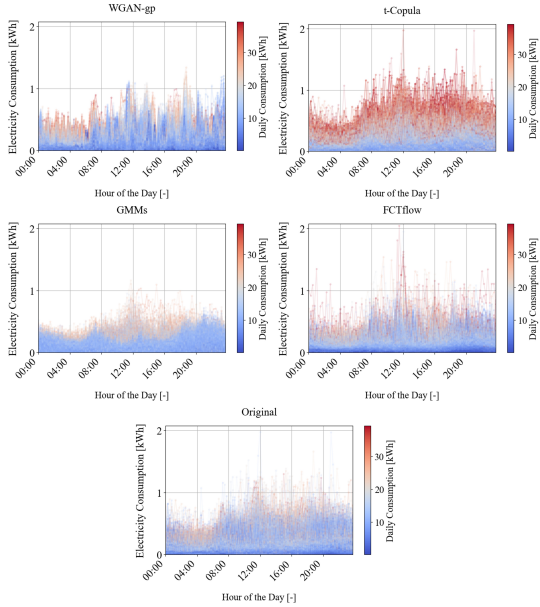


Fig. 5. The unconditional generation results of GMM, t-Copulas, WGAN-GP, and FCPFlow in the GE dataset. The color of the profiles represents the total daily consumption.

TABLE II
RESULTS OF EVALUATION METRICS FOR GE DATASET.

Model	ED	MSE.A	KS	WD	MMD
t-Copulas	0.1212	0.0134	0.2956	0.0624	0.0190
GMMs	0.0394	0.0224	0.0861	0.0168	0.0201
WGAN-GP	0.0543	0.0124	0.1527	0.0110	0.0237
FCPFlow	0.0372	0.0053	0.1057	0.0147	0.0068

2) Evaluation Metrics for RLP Probabilistic Prediction:

The evaluation metrics for the Sec. VII are Pinball loss (PL), Continuous Ranked Probability Score (CRPS), and the MSE between the true and the average of predicted profiles [21], [38]. Similarly, the smaller the value of these metrics, the better the prediction results of the model. The MSE is simply defined by the MSE of true value \mathbf{y}_t and the average of predicted value $\bar{\mathbf{y}}_p$. The PL function, used in quantile regression, is defined as

$$L_\tau(\mathbf{y}_t, \mathbf{y}_p) = \begin{cases} \tau(\mathbf{y}_t - \mathbf{y}_p) & \text{if } \mathbf{y}_t > \mathbf{y}_p \\ (1 - \tau)(\mathbf{y}_p - \mathbf{y}_t) & \text{otherwise,} \end{cases} \quad (33)$$

where y_p is the predicted RLP, τ is the quantile (e.g., 0.9 for the 9th percentile).

The CRPS is given by the integral of the squared difference between the CDF of the prediction and the observed value's CDF. The CRPS is expressed as

$$\text{CRPS}(F, \mathbf{y}_t) = \int_{-\infty}^{\infty} (F(\mathbf{y}_p) - \mathbb{1}(\mathbf{y}_p \geq \mathbf{y}_t))^2 d\mathbf{y}_p, \quad (34)$$

where $\text{CRPS}(F, \mathbf{y}_t)$ is the CRPS for a prediction distribution F , $F(\mathbf{y}_p)$ represents the CDF of the predicted distribution evaluated at \mathbf{y}_p , and $\mathbb{1}(\mathbf{y}_p \geq \mathbf{y}_t)$ is the indicator function, which equals 1 when $\mathbf{y}_p \geq \mathbf{y}_t$ and 0 otherwise.

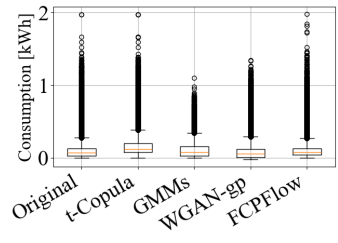


Fig. 6. Boxplot of the original and generated consumption values by four models using the GE dataset. Results show that the FCPFlow and Copulas models reproduce the original peak values.

VI. SIMULATION RESULTS FOR RLP GENERATION

A. Unconditional Generation

In this section, we first evaluate the performance of the proposed FCPFlow architecture on the unconditional generation task. Based on previous studies [26], [39] t-Copulas, GMM, and WGAN-GP are selected as benchmarks for comparison against FCPFlow. The GE dataset is used for comparison. Fig 5 shows the generated results. Table II summarizes the results of evaluation metrics, where we find that FCPFlow outperforms other models in the ED (decrease by 0.0022), MSE.A (decrease by 0.0071), and MMD (decrease by 0.0122) metrics, and rank the second position in KS and WD. This suggests its superiority in capturing temporal correlations. In contrast, GMM, although effective at modeling the population distribution (as shown by small ED and KS scores), falls short in modeling the correlation between time steps. In contrast, deep generative models like WGAN-GP and FCPFlow perform well in this regard. Further evidence of FCPFlow's ability to accurately replicate volatility in RLPs is provided by the boxplot in Fig 6, which shows that only Copulas and FCPFlow successfully reproduce the original peak values. Fig 5 reveals that t-Copulas tends to produce RLPs with higher daily consumption, as indicated by a greater number of RLPs with more intense red hues. This pattern, consistently observed across various experiments, may suggest that t-Copulas-generated RLPs exhibit less volatility (an RLP with relatively high consumption at the first time step tends to keep this high consumption pattern in the following time steps) compared to FCPFlow-generated RLPs and the original data.

B. Conditional Generation Based on Consumption

In this section, we test the FCPFlow's performance on conditional generation. The conditions used are annual consumption and daily consumption (in kWh) related to each RLP. Consequently, the FCPFlow model is formalized as $F(\mathbf{z}; c_{ann}, c_{daily})$. The datasets used are UK, AUS, NL, and USA which have different resolutions. Previous research by [26] has established that t-Copulas outperforms conditional GMMs in conditional RLP generation tasks. Therefore, our comparative analysis focuses on measuring the performance differences between FCPFlow and t-Copulas.

In these experiments, the datasets are split into a test set (20% of data) and a training set (80% of data). The models are first trained using the training dataset. Then, RLPs are

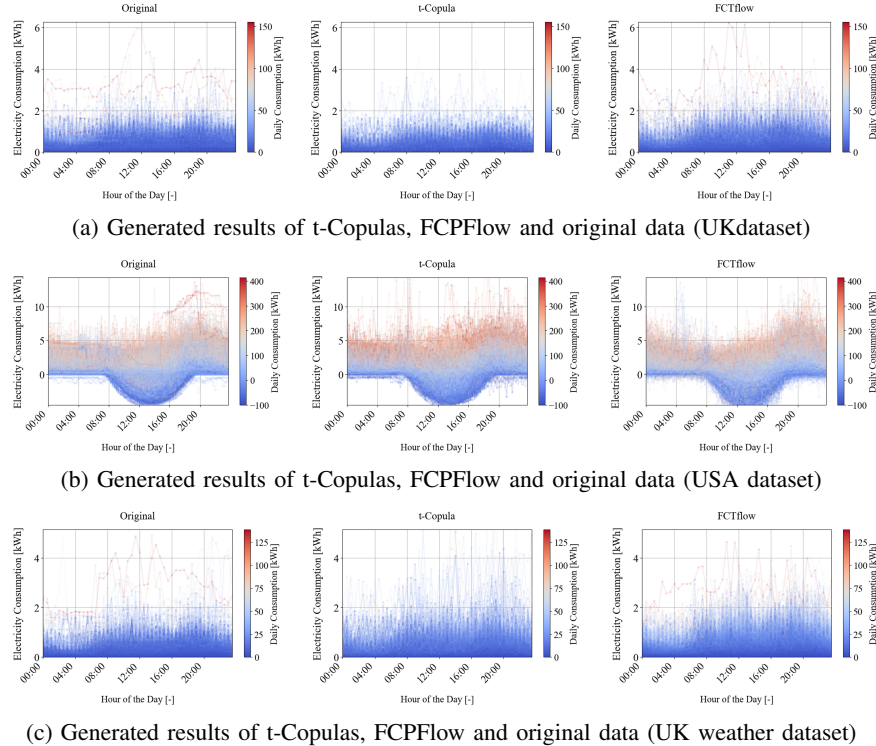


Fig. 7. The part of conditional generated results of t-Copulas and FCPFlow using UK, USA, and UK-weather datasets. The color of the profiles represents the total daily consumption.

generated according to the conditions specified in the test set. Finally, we compute the evaluation metrics by comparing these generated RLPs with the actual data in the test set.

Fig 7 (a-b) shows parts of the generated results, where we observe again that t-Copulas tend to produce RLPs with higher daily consumption, identifiable by the more vivid red colors. Interestingly, the FCPFlow model successfully generated outliers in the test dataset—the RLP with the highest peak. This RLP is the red curve with the maximum consumption peak (see 7(a)), t-Copulas fails to generate this RLP. In a more quantitative analysis, as shown in Table III, FCPFlow outperforms t-Copulas on most metrics across experiments, in which FCPFlow achieves the best MMD in four datasets (100%), and the best MSE.A and KS in three datasets (75%), the best ED in two datasets (50%). FCPFlow's superior performance in modeling correlations can be attributed to its lack of predefined assumptions, whereas t-Copulas relies on the assumption of using the Student-t distribution to model temporal correlations.

Another observation is that the performance of the t-Copulas model is highly dependent on the characteristics of the RLP datasets, a finding that echoes the research presented in [29]. The t-Copulas demonstrates superior performance with the UK dataset, closely matching FCPFlow in several metrics except for the MMD. In the USA dataset, t-Copula achieves a better overall performance. However, t-Copula struggles with the NL and GE datasets, which have a significant performance gap compared with the FCPFlow model. For example, the FCPFlow model achieves approximately two to three times better scores in the NL and GE datasets than the t-Copula model. This variation in performance can be attributed to the

TABLE III
RESULTS OF EVALUATION METRICS FOR NL, UK, AND USA DATASET.

Model	ED	MSE.A	KS	WD	MMD
NL 60 minute resolution					
t-Copulas	0.1896	0.0221	0.2831	0.1033	0.0473
FCPFlow	0.0650	0.0051	0.1546	0.0387	0.0150
UK 30 minute resolution					
t-Copulas	0.0064	0.0003	0.0192	0.0037	0.0048
FCPFlow	0.0052	0.0004	0.0106	0.0038	0.0006
AUS 30 minute resolution					
t-Copulas	0.0628	0.0037	0.1290	0.0389	0.0070
FCPFlow	0.0635	0.0013	0.1199	0.0463	0.0010
USA 15 minute resolution					
t-Copulas	0.0191	0.0019	0.0198	0.0315	0.0016
FCPFlow	0.0320	0.0017	0.0571	0.0601	0.0014

Copulas model's reliance on specific, predefined assumptions.

C. Conditional Generation Based on Weather

In this section, we examine the performance of FCPFlows using weather information as conditions. The dataset used is UK weather data with a 30-minute resolution. As previously done, the data set is divided into a training set (80% of the data) and a test set (the remaining 20%). Weather conditions considered in this analysis include cloud cover, sunlight, radiation, maximum temperature, minimum temperature, average temperature, pressure, and precipitation. The correlation analysis between total daily consumption and weather is shown in Fig 8. For this experiment, the FCPFlow model is represented as $F(\mathbf{z}; c_{ann}, c_{weather})$, where $c_{weather}$ contains eight specified weather features.

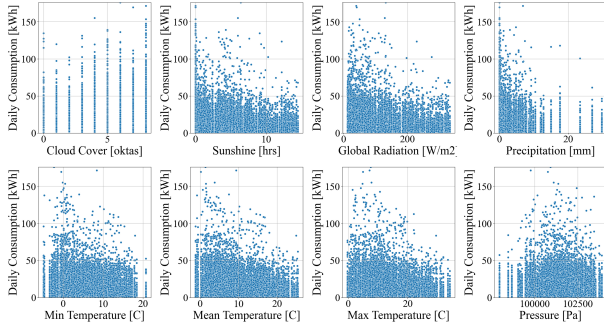


Fig. 8. The weather information includes cloud cover, sunshine, irradiation, maximum temperature, minimum temperature, mean temperature, pressure, and precipitation. The figures show the correlation of weather information with the daily total consumption.

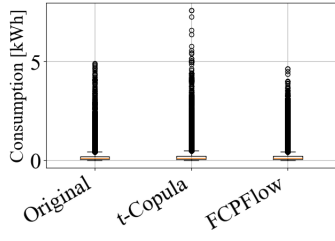


Fig. 9. Boxplot of the original and conditioned generated consumption values by two models (t-Copula and FCPFlow) using the UK weather dataset.

Fig 7 (c) shows the generated results. The results show again that FCPFlow replicates the RLPs with the highest peaks (the red curve with the highest peak) while t-Copulas fails to do so. A detailed quantitative analysis in Table IV shows that the FCPFlow model significantly outperforms the t-Copulas model. Specifically, enhancements include a reduction of 0.036 in ED, a reduction of 0.019 in MSE.A, and a reduction of 0.061 in WD. Fig 9 illustrates the trend of RLPs generated by t-Copulas towards higher consumption values. There may be two reasons for the worse results by the Copula model: 1) t-Copula assumes that the correlation of RLPs follows Student-t distribution, which may be different from reality, and 2) t-Copulas model in [26] relies on the empirical CDF to model the marginal distribution, this method allows t-Copulas to reproduce the marginal distribution of the training set perfectly, but it can also lead to overfitting, which negatively affects the accuracy of the model in representing peaks and correlations in the test set.

VII. SIMULATION RESULTS FOR RLP PROBABILISTIC PREDICTION

The developed FCPFlow model is also capable of RLP probabilistic prediction. In this section, we compare the FCPFlow model's performance with other state-of-the-art generative model-based load prediction methods, cVAE, cNICE, and cWGAN-GP. We use NL, USA, and UK datasets in Table I.

The NL, UK, and USA datasets are split into a test set (20% of data) and a training set (80% of data). All models are designed to take a complete RLP of the previous day as a condition and predict the RLP of the next day. Fig 10 shows a one-day example of profiles predicted by models.

TABLE IV
RESULTS OF EVALUATION METRICS FOR UK WEATHER DATASET.

Model	ED	MSE.A	KS	WD	MMD
t-Copulas	0.0306	0.0037	0.0356	0.0263	0.0024
FCPFlow	0.0267	0.0018	0.0487	0.0202	0.0072

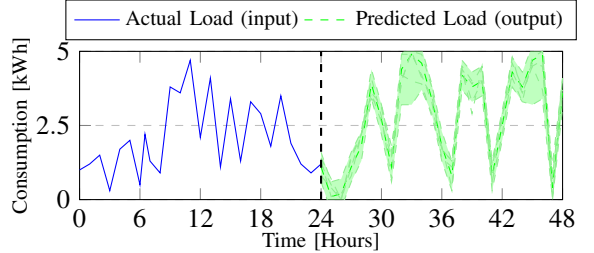


Fig. 10. All prediction models take the consumption profile of the first day and make probabilistic predictions for the second day. FCPFlow model can be expressed as $F(\mathbf{z}; c_d)$, where c_d represents the RLP of the previous day.

The evaluation metrics used are PL, CRPS, and MSE between the actual and average of predicted profiles, as introduced in Section V-C2. We use the average PL and CRPS over time steps.

Fig 11 illustrates the predictive outcomes. From Fig 11, we can observe that the FCPFlow model performs better in predicting critical aspects of the load, such as peaks, valleys, and volatility. Specifically, Fig 11(a) demonstrates the FCPFlow model's proficiency in accurately predicting most peaks, in contrast to cVAEA, which tends to overestimate, and cNICE, which generally predicts lower peak values. This pattern persists across other datasets. In the case of Fig 11(c), which represents the most volatile scenario, although all models struggle to predict the highest peak accurately, the FCPFlow model successfully predicts most of the remaining peaks and valleys.

Table V provides a comprehensive quantitative comparison across models, highlighting the superior performance of FCPFlow over similar models. Specifically, FCPFlow achieves the lowest MSE values on the NL and UK datasets, while on the US dataset, the MSE loss slightly lags behind cWGAN-GP. Furthermore, FCPFlow consistently exhibits significantly lower errors, ranging from 16% to 64% smaller PL errors and 5% to 46% smaller CRPS errors compared to other models. This analysis confirms the efficacy of FCPFlow not only in RLP generation but also as an advanced RLP probabilistic prediction method.

VIII. DISCUSSIONS

Fig 12 summarises the evaluation results of all experiments presented. The average scores for five conditional generation experiments (UK, AUS, USA, NL, UK Weather) are computed. To facilitate understanding, the smaller the area in Fig 12, the better the model's overall performance. Based on this, the FCPFlow generally performs better than all other models. In generating RLPs, deep learning models are good at capturing temporal correlations [29]. However, they often fall short of accurately reflecting the overall statistical properties,

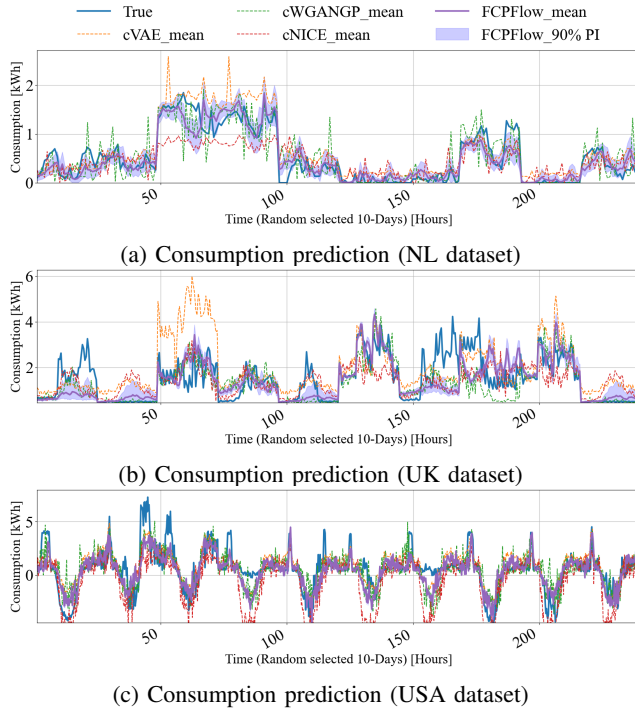


Fig. 11. RLP probabilistic prediction for three datasets NL, UK, and USA. Different colors represent the true observation and the average of predictions. The blue area represents the 90% prediction interval of the FCPFlow model.

TABLE V
RESULTS OF EVALUATION METRICS FOR PROBABILISTIC LOAD PREDICTION.

Model	PL	MSE	CRPS
<i>NL dataset 60 minute resolution</i>			
cVAE	0.1068	0.3616	0.4383
cWGANGP	0.1031	0.2302	0.4993
cNICE	0.1038	0.2406	0.5082
FCPFlow	0.0551	0.2052	0.4131
<i>UK dataset 30 minute resolution</i>			
cVAE	0.0884	1.1491	1.6134
cWGANGP	0.1093	0.5511	2.0100
cNICE	0.1210	0.6913	2.8822
FCPFlow	0.0427	0.5412	1.5326
<i>USA dataset 15 minute resolution</i>			
cVAE	0.2306	0.7838	1.1609
cWGANGP	0.2283	0.4865	1.064
cNICE	0.2846	0.7177	1.396
FCPFlow	0.1911	0.4913	0.8799

such as mean and variance. This limitation stems from the fact that models like GAN and VAE do not inherently model probability densities directly. Flow-based models address this limitation by explicitly approximating the probability density since the optimization of flow-based models responds to *Change of Variable Theorem* expressed in (3), thereby ensuring that overall statistical characteristics are better captured. Despite their strengths, traditional flow-based models have lacked the modeling capabilities seen in other deep generative models. This is because conventional flow-based models have to ensure invertibility. Therefore, flow-based models are not as flexible as other generative models. The proposed FCPFlow model retains the probabilistic precision of flow-based models while enhancing their modeling capacities for RLP data by introduc-

ing invertible linear layers and invertible normalization layers. Therefore, the FCPFlow model shows excellent performance in simultaneously capturing the temporal correlation and overall statistical characteristics of RLPs.

Copulas models offer the benefits of quick modeling and a relatively robust capabilities, especially for smaller datasets, as highlighted by [26]. However, its assumptions constrain its performance, leading to challenges in accurately modeling complex correlations across different time steps. This limitation becomes apparent in our experiments, where Copulas' effectiveness varies, particularly with the GE and NL datasets. Additionally, our findings suggest that Copulas may struggle to capture the high-dimensional features of RLPs, as evidenced by consistently high MMD values. As discussed in Sections VI-A to VI-B, Copulas tends to generate RLPs of higher daily consumption and less volatility, failing to capture the full spectrum of high-dimensional characteristics. These observations suggest that traditional metrics like WD, ED, and KS, may not adequately convey the fidelity of generated RLPs.

IX. CONCLUSION

This paper introduced the FCPFlow model, a novel flow-based architecture tailored to RLPs generation and probabilistic prediction. We conducted extensive experiments to evaluate FCPFlow's efficacy in three key areas: unconditional RLP generation (benchmarking against t-Copulas, GMMs, and WGAN-GP), conditional RLP generation (benchmarking against t-Copula), and RLP probabilistic prediction (benchmarking against cVAE, cWGANGP, and cNICE). The FCPFlow model exhibits superior performance across all tested scenarios. Notably, the FCPFlow model combines the strengths of deep generative models, such as high stability and effectiveness in capturing temporal correlations and high-dimensional features, but also excelling in modeling overall statistical features, as evidenced by low ED, WD, and KS, among others.

REFERENCES

- [1] S. Shao, M. Pipattanasomporn, and S. Rahman, "Development of physical-based demand response-enabled residential load models," *IEEE Transactions on power systems*, vol. 28, no. 2, pp. 607–614, 2012.
- [2] S. Krauter, "Simple and effective methods to match photovoltaic power generation to the grid load profile for a pv based energy system," *Solar Energy*, vol. 159, pp. 768–776, 2018.
- [3] E. M. S. Duque, J. S. Giraldo, P. P. Vergara, P. H. Nguyen, A. van der Molen, and J. Slootweg, "Risk-aware operating regions for pv-rich distribution networks considering irradiance variability," *IEEE Transactions on Sustainable Energy*, 2023.
- [4] P. McDaniel and S. McLaughlin, "Security and privacy challenges in the smart grid," *IEEE security & privacy*, vol. 7, no. 3, pp. 75–77, 2009.
- [5] W. Zomerdijk, P. Palensky, T. AlSkaif, and P. P. Vergara, "On future power systems digital twins: Towards a standard architecture," *arXiv preprint arXiv:2404.02568*, 2024.
- [6] F. Lombardi, S. Balderrama, S. Quoilin, and E. Colombo, "Generating high-resolution multi-energy load profiles for remote areas with an open-source stochastic model," *Energy*, vol. 177, pp. 433–444, 2019.
- [7] D. Zhou, S. Ma, J. Hao, D. Han, D. Huang, S. Yan, and T. Li, "An electricity load forecasting model for integrated energy system based on bigan and transfer learning," *Energy Reports*, vol. 6, pp. 3446–3461, 2020.
- [8] J. Francou, D. Calogine, O. Chau, M. David, and P. Lauret, "Expanding variety of non-intrusive load monitoring training data: Introducing and benchmarking a novel data augmentation technique," *Sustainable Energy, Grids and Networks*, vol. 35, p. 101142, 2023.

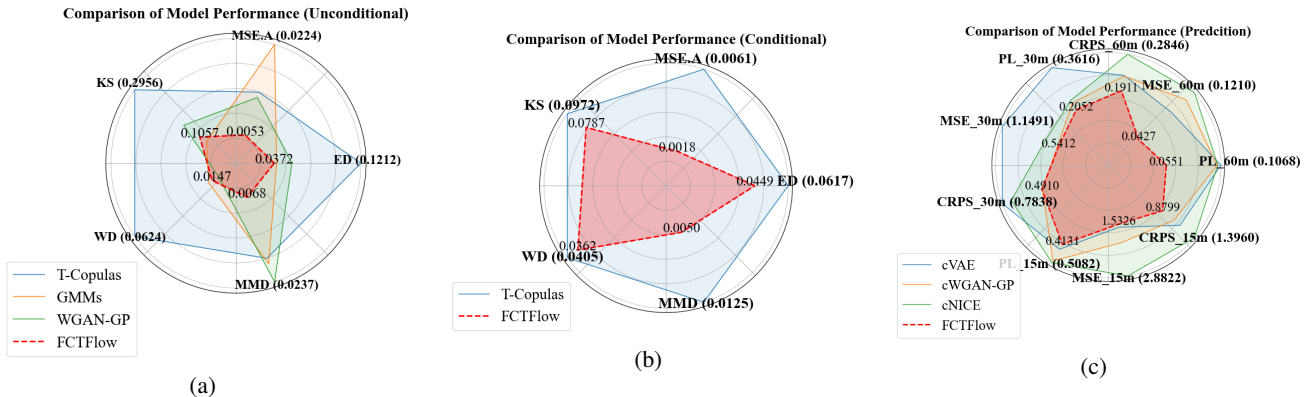


Fig. 12. A summary of evaluation results of all experiments. Figure (a) is for unconditional generation (GE), figure (b) is for conditional generation, and figure (c) is for load prediction. The average scores for five conditional generation experiments (UK, AUS, USA, NL, UK Weather) are computed and used for plotting. The smaller the area, the better the overall performance. Additionally, the metrics are normalized.

- [9] C. Zhang, S. R. Kuppannagari, C. Xiong, R. Kannan, and V. K. Prasanna, “A cooperative multi-agent deep reinforcement learning framework for real-time residential load scheduling,” in *Proceedings of the International Conference on Internet of Things Design and Implementation*, 2019, pp. 59–69.
- [10] R. Singh, B. C. Pal, and R. A. Jabr, “Statistical representation of distribution system loads using gaussian mixture model,” *IEEE Transactions on Power Systems*, vol. 25, no. 1, pp. 29–37, 2009.
- [11] R. Bernards, J. Moren, and H. Slootweg, “Statistical modelling of load profiles incorporating correlations using copula,” in *2017 IEEE PES Innovative Smart Grid Technologies Conference Europe (ISGT-Europe)*. IEEE, 2017, pp. 1–6.
- [12] J. Einolander and R. Lahdelma, “Multivariate copula procedure for electric vehicle charging event simulation,” *Energy*, vol. 238, p. 121718, 2022.
- [13] Y. Gu, Q. Chen, K. Liu, L. Xie, and C. Kang, “Gan-based model for residential load generation considering typical consumption patterns,” in *2019 IEEE Power & Energy Society Innovative Smart Grid Technologies Conference (ISGT)*. IEEE, 2019, pp. 1–5.
- [14] M. N. Fekri, A. M. Ghosh, and K. Grolinger, “Generating energy data for machine learning with recurrent generative adversarial networks,” *Energies*, vol. 13, no. 1, p. 130, 2019.
- [15] Z. Pan, J. Wang, W. Liao, H. Chen, D. Yuan, W. Zhu, X. Fang, and Z. Zhu, “Data-driven ev load profiles generation using a variational autoencoder,” *Energies*, vol. 12, no. 5, p. 849, 2019.
- [16] L. Ge, W. Liao, S. Wang, B. Bak-Jensen, and J. R. Pillai, “Modeling daily load profiles of distribution network for scenario generation using flow-based generative network,” *IEEE Access*, vol. 8, pp. 77 587–77 597, 2020.
- [17] M. Razghandi, H. Zhou, M. Erol-Kantarci, and D. Turgut, “Smart home energy management: Vae-gan synthetic dataset generator and q-learning,” *IEEE Transactions on Smart Grid*, 2023.
- [18] J. Huang, Q. Huang, G. Mou, and C. Wu, “Dpwgan: high-quality load profiles synthesis with differential privacy guarantees,” *IEEE Transactions on Smart Grid*, 2022.
- [19] W. N. Silva, L. H. Bandória, B. H. Dias, M. C. de Almeida, and L. W. de Oliveira, “Generating realistic load profiles in smart grids: An approach based on nonlinear independent component estimation (nice) and convolutional layers,” *Applied Energy*, vol. 351, p. 121902, 2023.
- [20] Y. Hu, Y. Li, L. Song, H. P. Lee, P. Rehm, M. Makdad, E. Miller, and N. Lu, “Multiload-gan: A gan-based synthetic load group generation method considering spatial-temporal correlations,” *IEEE Transactions on Smart Grid*, 2023.
- [21] Y. Wang, G. Hug, Z. Liu, and N. Zhang, “Modeling load forecast uncertainty using generative adversarial networks,” *Electric Power Systems Research*, vol. 189, p. 106732, 2020.
- [22] L. Song, Y. Li, and N. Lu, “Profilesr-gan: A gan based super-resolution method for generating high-resolution load profiles,” *IEEE Transactions on Smart Grid*, vol. 13, no. 4, pp. 3278–3289, 2022.
- [23] C. Wang, E. Sharifnia, Z. Gao, S. H. Tindemans, and P. Palensky, “Generating multivariate load states using a conditional variational autoencoder,” *Electric Power Systems Research*, vol. 213, p. 108603, 2022.
- [24] C. Fan, M. Chen, R. Tang, and J. Wang, “A novel deep generative modeling-based data augmentation strategy for improving short-term building energy predictions,” in *Building Simulation*, vol. 15. Springer, 2022, pp. 197–211.
- [25] L. Lin, C. Chen, B. Wei, H. Li, J. Shi, J. Zhang, and N. Huang, “Residential electricity load scenario prediction based on transferable flow generation model,” *Journal of Electrical Engineering & Technology*, vol. 18, no. 1, pp. 99–109, 2023.
- [26] E. M. S. Duque, P. P. Vergara, P. H. Nguyen, A. van der Molen, and J. G. Slootweg, “Conditional multivariate elliptical copulas to model residential load profiles from smart meter data,” *IEEE Transactions on Smart Grid*, vol. 12, no. 5, pp. 4280–4294, 2021.
- [27] X. Ding, Y. Wang, Z. Xu, W. J. Welch, and Z. J. Wang, “Ccgan: Continuous conditional generative adversarial networks for image generation,” in *International conference on learning representations*, 2020.
- [28] A. Heyrani Nobari, W. Chen, and F. Ahmed, “Pcdgan: A continuous conditional diverse generative adversarial network for inverse design,” in *Proceedings of the 27th ACM SIGKDD conference on knowledge discovery & data mining*, 2021, pp. 606–616.
- [29] W. Xia, H. Huang, E. M. S. Duque, S. Hou, P. Palensky, and P. P. Vergara, “Comparative assessment of generative models for transformer- and consumer-level load profiles generation,” *Sustainable Energy, Grids and Networks*, p. 101338, 2024.
- [30] G. Papamakarios, E. Nalisnick, D. J. Rezende, S. Mohamed, and B. Lakshminarayanan, “Normalizing flows for probabilistic modeling and inference,” *The Journal of Machine Learning Research*, vol. 22, no. 1, pp. 2617–2680, 2021.
- [31] D. Rezende and S. Mohamed, “Variational inference with normalizing flows,” in *International conference on machine learning*. PMLR, 2015, pp. 1530–1538.
- [32] L. Weng, “Flow-based deep generative models,” *lilianweng.github.io*, 2018. [Online]. Available: <https://lilianweng.github.io/posts/2018-10-13-flow-models/>
- [33] L. Dinh, D. Krueger, and Y. Bengio, “Nice: Non-linear independent components estimation,” *arXiv preprint arXiv:1410.8516*, 2014.
- [34] L. Ardizzone, C. Lüth, J. Kruse, C. Rother, and U. Köthe, “Guided image generation with conditional invertible neural networks,” *arXiv preprint arXiv:1907.02392*, 2019.
- [35] “Smart-Grid Smart-City Customer Trial Data - Electricity Use Interval Reading,” <https://data.gov.au/dataset/smart-grid-smart-city-customer-trial-data/resource/b71eb954-196a-4901-82fd-69b17f88521e>, Oct 2015.
- [36] Pecan Street Inc., “Dataport academic access,” <https://dataport.pecanstreet.org/academic>, 2023, accessed: [insert date of access].
- [37] E. Fwerr, “London weather data,” <https://www.kaggle.com/datasets/emmanuelfwerr/london-weather-data>, 2023, accessed: [insert date of access].
- [38] L. Zhang and B. Zhang, “Scenario forecasting of residential load profiles,” *IEEE Journal on Selected Areas in Communications*, vol. 38, no. 1, pp. 84–95, 2019.
- [39] N. Huang, Q. He, J. Qi, Q. Hu, R. Wang, G. Cai, and D. Yang, “Multinodes interval electric vehicle day-ahead charging load forecasting based on joint adversarial generation,” *International Journal of Electrical Power & Energy Systems*, vol. 143, p. 108404, 2022.